INTERNATIONAL
JOURNAL
of
SPINE
SURGERY

Biomechanical evaluation of a spherical lumbar interbody device at varying levels of subsidence

Steven A. Rundell, Jorge E. Isaza and Steven M. Kurtz

This information is current as of May 5, 2025.

Email Alerts	Receive free email-alerts when new articles cite this article. Sign up at: http://ijssurgery.com/alerts

INTERNATIONAL
SOCIETY *for the* ADVANCEMENT *of*
SPINE SURGERY

Biomechanics

Biomechanical evaluation of a spherical lumbar interbody device at varying levels of subsidence

Steven A. Rundell, MS [a,b,]*, Jorge E. Isaza, MD [c], Steven M. Kurtz, PhD [a,b]

[a] *Exponent, Inc, Philadelphia, PA*
[b] *Drexel University, Philadelphia, PA*
[c] *Tulane University, New Orleans, LA*

Background: Ulf Fernström implanted stainless steel ball bearings following discectomy, or for painful disc disease, and termed this procedure disc arthroplasty. Today, spherical interbody spacers are clinically available, but there is a paucity of associated biomechanical testing. The primary objective of the current study was to evaluate the biomechanics of a spherical interbody implant. It was hypothesized that implantation of a spherical interbody implant, with combined subsidence into the vertebral bodies, would result in similar ranges of motion (RoM) and facet contact forces (FCFs) when compared with an intact condition. A secondary objective of this study was to determine the effect of using a polyetheretherketone (PEEK) versus a cobalt chrome (CoCr) implant on vertebral body strains. We hypothesized that the material selection would have a negligible effect on vertebral body strains since both materials have elastic moduli substantially greater than the annulus.
Methods: A finite element model of L3-L4 was created and validated by use of ROM, disc pressure, and bony strain from previously published data. Virtual implantation of a spherical interbody device was performed with 0, 2, and 4 mm of subsidence. The model was exercised in compression, flexion, extension, axial rotation, and lateral bending. The ROM, vertebral body effective (von Mises) strain, and FCFs were reported.
Results: Implantation of a PEEK implant resulted in slightly lower strain maxima when compared with a CoCr implant. For both materials, the peak strain experienced by the underlying bone was reduced with increasing subsidence. All levels of subsidence resulted in ROM and FCFs similar to the intact model.
Conclusions: The results suggest that a simple spherical implant design is able to maintain segmental ROM and provide minimal differences in FCFs. Large areas of von Mises strain maxima were generated in the bone adjacent to the implant regardless of whether the implant was PEEK or CoCr.
© 2011 SAS - The International Society for the Advancement of Spine Surgery. Published by Elsevier Inc. All rights reserved.

Keywords: Lumbar; Finite element; Spine biomechanics; Arthroplasty; Subsidence; Facet contact

Despite the resurgent interest in lumbar disc arthroplasty, these procedures were initially performed in the 1960s. Ulf Fernström implanted stainless steel ball bearings after discectomy, or for painful disc disease, and termed this procedure "disc arthroplasty."[1] At that time, persistent low-back pain was prevalent after discectomy of a herniated or painful disc. Whereas combining discectomy with fusion improved clinical results, there was an increased risk of infection, pseudarthrosis, thrombosis, embolus, and death.[2] More recently, fusion has been associated with adjacent-level disc degeneration, which may be the result of an altered biomechanical environment.[3–5] Therefore Fernström introduced a type of arthroplasty involving implantation of a spherical endoprosthesis (stainless steel ball bearing) into the center of an evacuated disc. The intention of such a procedure was to provide a motion-preserving alternative to fusion, which would potentially prevent or forestall degenerative changes at the adjacent levels.

The Fernström prosthesis has been criticized for having a high subsidence risk.[6,7] Subsidence has also recently been documented as a complication after modern total disc replacements (TDRs) for both mobile and fixed-core implants.[8–10] However, very few biomechanical studies have been performed to determine the cause and factors associated with TDR subsidence. Two-year follow-up performed by Fernström[1] showed indentation of the implant into the endplates ranging from 1 to 3 mm. Two-year clinical follow-up of a modern, fixed-core TDR implanted in athletes showed 2 to 3 mm of subsidence of the implants in 30% of

---

* Corresponding author: Steven A. Rundell, MS, Exponent, Inc, 39100 Country Club Dr, Farmington Hills, MI 48331; Tel: (248) 324-9158; Fax: (248) 324-9199.

E-mail address: srundell@exponent.com

the patients occurring during the first 3 months.[11] For this modern TDR design, up to 5 mm of subsidence was considered "minor" and was not judged to have an adverse effect on the clinical outcome. A different study involving a modern, elastomeric nucleus replacement documented endplate changes after implantation, which the authors attributed to loading of the endplate by the implant.[12] Despite these endplate changes, the authors documented favorable clinical results in 88% of their patients after 1 to 2 years. Thus several contemporary studies indicate that the levels of subsidence documented by Fernström are also observed with modern spinal arthroplasty technologies. Furthermore, initial subsidence of disc arthroplasty devices may be unavoidable and does not appear to necessarily predict poor clinical results, provided that the subsidence equilibrates after an initial period without further, long-term unstable loss of disc height or neural foramina. Fernström indicated that indentation of the implant into the endplate prevented ventral and dorsal slipping while still allowing bending movements, suggesting that initial subsidence of the device may improve its functionality.

Complications reported by Fernström[1] included expulsion of the device in 1 case (0.7%) and temporary paresis of the peroneus in another case (0.7%) after 2 years. Interestingly, there were no observations made regarding the facets at the index level. However, a later clinical study that evaluated spherical interbody implants after 10 to 20 years of implantation reported the need for subsequent fusion as a result of facet arthrosis in 10% of patients treated for degenerated disc disease and in none of those treated for a protruding disc.[13] In modern fixed or mobile-bearing TDRs, facet arthrosis at the implanted level may occur in approximately one-third of the patients after 3 years regardless of TDR type.[14] Several contemporary studies have also documented that facet joint triggered low-back pain as a complication associated with modern TDRs.[11,15,16] It is unclear what contributes to the prevalence of facet arthrosis after TDR, and this is further complicated by the difficulty in diagnosing the disease in its early stages. However, several studies have hypothesized or showed altered facet loading after implantation of modern TDRs,[17–22] which may be attributed to changes in the center of rotation or removal of associated soft-tissue structures, such as the anterior longitudinal ligament (ALL) and most of the annulus. Because the Fernström prosthesis can be implanted without resection of the ALL, and the center of rotation will inherently be near the center of the disc, loading in the facets may be similar to the preimplanted condition. However, no biomechanical studies have quantified facet loading after implantation of a spherical interbody device.

Long-term follow-up of patients implanted with a Fernström sphere was performed at 10 to 20 years by McKenzie.[13] He reported good or excellent clinical outcomes in 83% of patients treated for disc protrusions and 75% of those treated for disc pain. These results are similar to a recent clinical study involving a contemporary, mobile-bearing disc arthroplasty, which indicated good or excellent results in 82% of patients approximately 13 years after implantation.[10] Despite certain similarities in clinical outcomes between the Fernström sphere and modern technologies, the device has not been widely used clinically. Today, spherical interbody spacers fabricated from polyetheretherketone (PEEK) or cobalt-chrome alloy (CoCr) are clinically available; however, a paucity of clinical and biomechanical data remain for these devices.

The primary objective of this study was to evaluate the biomechanics of a spherical interbody implant by use of a previously validated finite element model (FEM) of a single lumbar motion segment. It was hypothesized that implantation of a spherical interbody implant, with combined subsidence into the vertebral bodies, would result in similar ranges of motion (ROMs) and facet contact forces (FCFs) when compared with an intact condition. A secondary objective of this study was to determine the effect of using a PEEK implant versus a CoCr implant on vertebral body strains. We hypothesized that the material selection would have a negligible effect on vertebral body strains because both materials have elastic moduli substantially greater than the annulus.

Methods

A 3-dimensional FEM of a ligamentous L3-4 motion segment was generated from quantitative computed tomography (QCT) data of a cadaveric spine. The donor was a 78-year-old man who died of cardiac arrhythmia. The data set was taken from an institutional review board–approved cadaveric study. The spine was chosen because of its lack of any bony or disc deformities (ie, osteophytes, herniations, or degenerative disc disease). Hounsfield units were used as a surrogate for bone mineral density (BMD). Elastic moduli within the vertebral body fell within what has been previously reported in the literature.[23–25] The development of the model has been previously described but will be outlined later.[22] A combination of automatic and manual image segmentation techniques (Analyze; AnalyzeDirect, Inc, Lenexa, Kansas) were used to extract detailed surfaces corresponding to the major bony structures of L3-4. The software package allowed for automatic segmentation based on thresholding of the QCT grayscale values. These surfaces were imported into the commercial finite element mesh–generation program HyperMesh (Altair Inc, Troy, Michigan) and were discretized into a combination of tetrahedral elements for the bony structures and hexahedral elements for the intervertebral disc. The central portion of the IVD, approximately 40% of the volume,[26] was designated to be the nucleus pulposus, whereas the remaining volume was considered the annulus fibrosus. Major spinal ligaments (ALL posterior longitudinal ligament, infraspinatus, supraspinatus, intratransverse ligament, facet capsule, and ligamentum flavum) were implemented in the model by use of tension-only nonlinear springs. Shell elements were used to
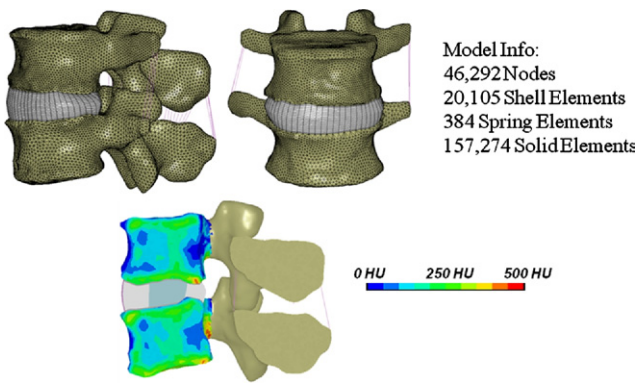
Fig. 1. Three-dimensional FEM of ligamentous L3-4 motion segment. A sagittal cross section depicts the contours of Hounsfield units (HU), which were used as a surrogate for BMD.
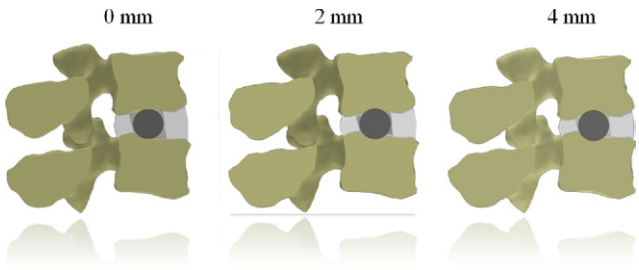

Fig. 2. Fernström spheres were virtually implanted to depict 3 levels of subsidence. Sagittal cross-sections of the 3 models are shown: 0 mm of implant subsidence (left), 2 mm of implant subsidence (center), and 4 mm of implant subsidence (right).

plate the exterior surface of the vertebral bodies and represented the cortex and bony endplate (Fig. 1). A refinement study was performed to determine the appropriate level of discretization.

BMD-dependent orthotropic material properties were assigned to the cancellous bone of the vertebral bodies. Custom software was written to apply the measured Hounsfield numbers from the QCT data to the nodal points within the finite element mesh. Similar methodology has been used to create models with heterogeneous bone properties of the tibia and femur.[27,28] The quantitative relationship between BMD and elastic modulus in cancellous vertebral bone, as reported by Ulrich et al[29] and Morgan et al,[30] was used to define a nonlinear relationship between BMD and orthotropic elastic modulus. Elastic moduli within the vertebral body fell within what has been previously reported in the literature.[23–25] The remaining structures were assigned material properties from the literature and are depicted in Table 1. Frictionless contact was defined between the facets by use of a penalty-based contact algorithm.

Two separate analyses were performed to validate the results of the model. The first analysis involved applying a 1,000-N compressive force to the intact model to simulate previously published experiments using cadaveric speci-mens.[39] The total vertical displacement of L3, intervertebral disc pressure, and cortical and endplate first principal strains were compared between the FEM and the previously published experimental data.[39] A second validation study was performed by applying moments of 7.5 N-m along the 3 principal anatomic axes and comparing total ROM in flexion-extension, lateral bending, and axial rotation with previously published data.[40–45]

A virtual implantation of a 16-mm-diameter sphere was performed on the intact model, which resulted in a total distraction of 4 mm. The 16-mm-diameter sphere was chosen to simulate subsidence of the implant of 2 mm into each endplate without reducing the total disc height beyond the intact state (12 mm). To simulate subsidence, 2 additional models were created with total subsidence of the implant into the vertebral bodies of 2 and 4 mm distributed equally between the superior and inferior endplates (Fig. 2). The initial forces and stresses in the annulus and ligaments were set to 0 at the fully distracted state for all models. This was done to isolate the effect of facet joint distraction and endplate-implant loading for different levels of subsidence. Subsidence of the implant was applied symmetrically between the inferior and superior endplate. The nucleus and cartilaginous endplate were removed within the nuclear cavity. For the cases of 2 and 4 mm of subsidence, vertebral bone was removed to accommodate for the implant geometry. A layer of shell elements representing the bony end-

Table 1
Summary of element type and material properties used in FEM

Component	Element type	Thickness or cross-sectional area	Young modulus (MPa)/ Stiffness Parameter	Poisson ratio
Cortical bone[31]	Shell	0.4 mm	12,000	0.3
Vertebral endplate[32]	Shell	0.25 mm	1,000	0.2
Cancellous bone[29,30]	Tet	N/A	$4,730\rho^{1.56}/1,987\rho^{1.56}/1,357\rho^{1.56}$	0.2
Posterior elements[33]	Tet	N/A	3,500	0.25
Annulus fibrosus ground substance[34]	Hex	N/A	1.36	0.45
Annulus fibrosus collagen fibers[35]	Fabric	N/A	Stress-strain curve	
Nucleus pulposus[31]	Hex	N/A	K = 1,666.7	Incompressible
Ligaments[36,37]	Spring	N/A	Hyperelastic	N/A
Cartilage endplate[38]	8-Noded hex	N/A	24	0.4

Abbervations: Tet, Tetrahedron; Hex, hexahedron; NA, not available.

plate was maintained between the implant and vertebral body at all levels of subsidence. The heterogeneous modulus of the underlying cancellous bone was not altered for the different levels of subsidence. Frictionless contact was defined at the implant-endplate interfaces as well as between the implant and the interior surface of the annulus fibrosus. To determine the sensitivity to friction, both flexion and extension were applied to the model with 4 mm of subsidence with a coefficient of friction of 0.5. These results indicated a less than 10% difference in the total flexion-extension ROM when compared with the frictionless model. The spherical implant was modeled by use of material properties for PEEK (Young's Modulus = 4 GPa, Poisson's Ratio = 0.46) and CoCr (Young's Modulus = 200 GPa, Poisson's Ratio = 0.3).

A compressive follower load of 500 N was applied to the intact model and implanted with 0 mm of subsidence, 2 mm of subsidence, and 4 mm of subsidence with both a PEEK and CoCr implant. A combination of a compressive follower load (500 N) and flexion (7.5 N-m), extension (7.5 N-m), lateral bending (7.5 N-m), and axial rotation (7.5 N-m) was applied to all models with the implant modeled as PEEK. Rotational loading was applied via a moment at the center of mass of the superior endplate of L3, which was modeled as a rigid body. There were no constraints applied to any of the rotational or translational degrees of freedom of the L3 superior endplate. The inferior endplate of L4 was constrained in all degrees of freedom to provide an appropriate boundary condition. All models were solved by use of the commercial FEM software program LS-Dyna (LSTC, Livermore, California).

Vertebral body cancellous bone effective (von Mises) strains were determined. Strain was chosen over stress because of the heterogeneous nature of the vertebral bone. Strain has been documented to have less dependence on the apparent density when compared with stress.[23] von Mises strain was chosen to depict the distortional strain being experienced in the vertebral bodies after implantation of a spherical implant. von Mises yield criterion is often used to predict the yield point for bone.[46] The von Mises strain is intended to qualitatively depict areas of the bone that may be most at risk of yielding after device implantation. ROM was defined as the total angular rotation of L3. The total FCF was defined as the sum of all nodal contact forces for both the left and right facet.

Results

In our validation analyses the model was generally able to predict cortical and endplate strains within the ranges reported in the literature.[39] Typically, the model's results matched the trends shown by the experimental median values (Fig. 3). In addition, the model predicted a disc pressure of 0.75 MPa and a total vertical displacement of 1.1 mm after application of 1,000 N of compression, which fell within the range of the experimentally reported values.
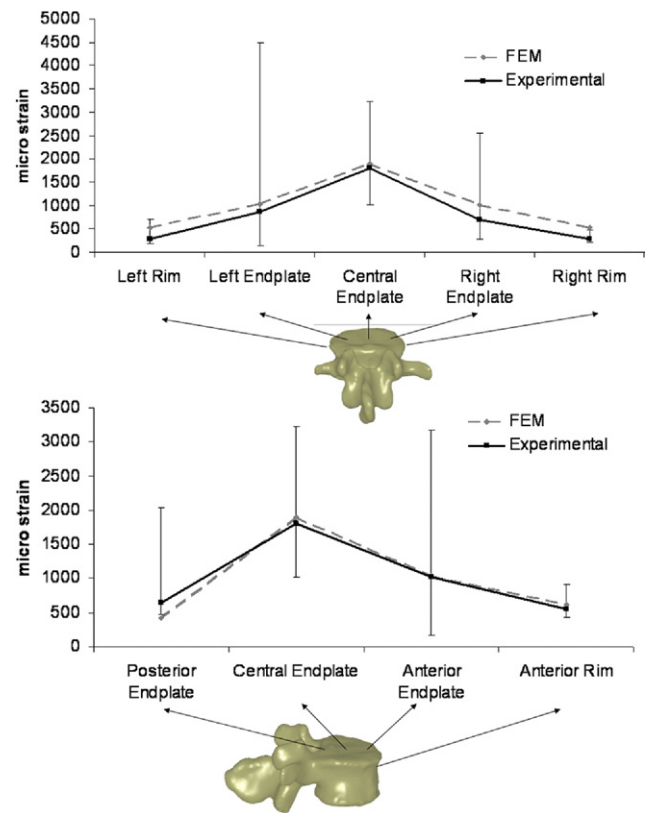

Fig. 3. Graphs depicting first principal strains at various locations along endplate and cortical rim between previously published experimental (Frei et al[39]) and FEM results.

Further validation indicated that the model predicted the total ROM in flexion-extension, lateral bending, and axial rotation (Fig. 4).

When we analyzed the Fernström prosthesis, peak effective strain in the cancellous bone during compression occurred just beneath the surface adjacent to the endplate-implant interface, with values of 0.48%, 12.9%, and 14.7% for the intact model, model implanted with PEEK and 0 mm of subsidence, and model implanted with CoCr and 0 mm of subsidence, respectively. Peak effective strain reduced to 4.0% and 4.6% at 2 mm of subsidence for the PEEK and CoCr implants, respectively. At 4 mm of subsidence, the peak effective strain was 2.7% and 3.0% for the PEEK and CoCr implants, respectively. Compressive loading resulted in strain maxima at the implant-endplate interface for both CoCr and PEEK implants (Fig. 5). Qualitatively, the PEEK implant resulted in a slight decrease in the size of the strain maxima. Both the PEEK and CoCr implants resulted in a decrease in strain maxima with increasing subsidence. During 0 mm of subsidence, the strain maxima occurred directly adjacent to the implant. At 2 mm of subsidence, the strain maxima in the superior vertebrae radiated out from the anterior and posterior portions of the endplate-implant interface, which resulted in an area of reduced strain maxima near the most superior portion of the implant. At 4 mm of subsidence, the strain maxima occurred at the anterior and
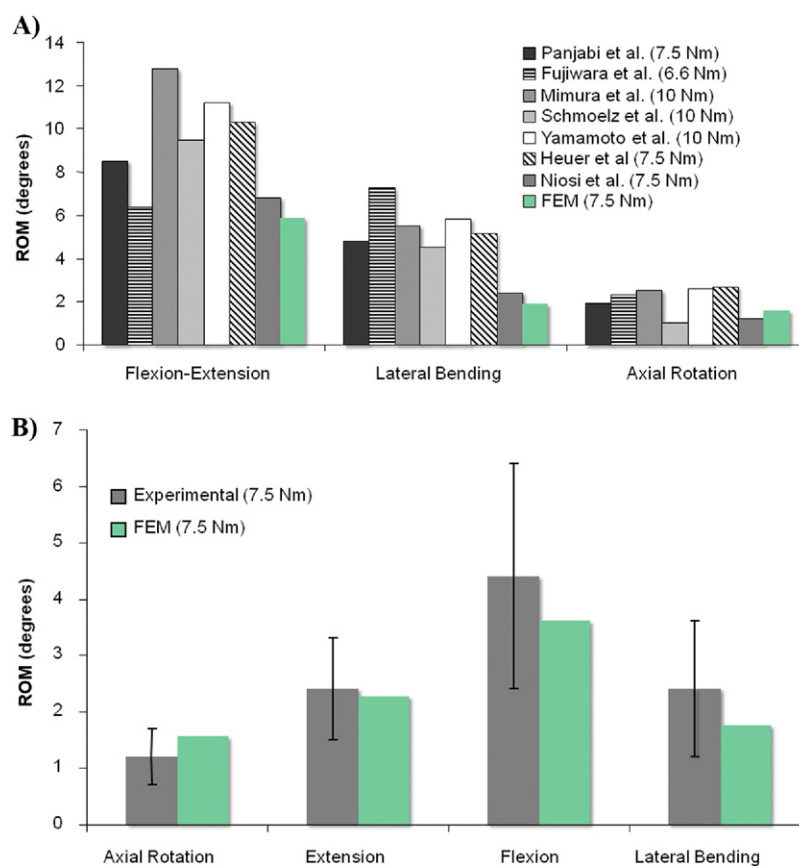
Fig. 4. A, Bar graph depicting comparison of angular ROM between FEM versus several previously published values (Heuer et al[37], Yamamoto et al[40], Mimura et al[41], Panjabi et al[42], Fujiwara at al[43], Schmoelz et al[44], Niosi et al[45]). B, Bar graph showing comparison between FEM and a specific set of experimental data (Niosi et al[45]), which also includes ranges for the SDs.

posterior portions of the endplate-implant interface in both the superior and inferior vertebral bodies.

Increased subsidence of the device from 0 to 4 mm resulted in a progressive decrease of the ROM (Fig. 6A). Implantation with 0 mm of subsidence resulted in increased ROM for all modes of loading compared with the intact model. These increases ranged from 80% during axial rotation to 10% during flexion (Tables 2 and 3). Subsidence of 2 mm resulted in increased ROM for all modes of loading with the exception of flexion. The increased ROM during 2 mm of subsidence was greatest during extension (31%). Subsidence of the implant at 4 mm resulted in decreased ROM for all modes of loading when compared with the intact model, from −32% to −3%.

FCFs in the intact model were greatest during axial rotation (148 N), lesser in extension (77 N), and least during lateral bending (22.5 N). Flexion resulted in distraction of the facets for both the implanted and intact models. FCFs tended to increase with increasing subsidence of the device from 0 to 4 mm (Fig. 6B). Zero millimeters of subsidence resulted in a decreased FCF for all modes of loading between −16% and −48% when compared with the intact model (Table 3). Two millimeters of subsidence resulted in a small increase in FCF during axial rotation (3%) but decreased FCF during extension (−35%) and lateral bend-

ing (−37%) when compared with the intact model. FCFs increased at 4 mm of subsidence for all modes of loading between 9% and 34% when compared with the intact model.

Contours of von Mises strain in the cancellous bone of the vertebral bodies indicated values below 1% for the intact model with the exception of a small area near the ALL attachment during extension (Fig. 7). Implantation of a PEEK spherical implant resulted in increased strain maxima adjacent to the implant-endplate interface for all modes of loading and levels of subsidence. Qualitatively, areas of strain maxima tended to decrease with increasing levels of implant subsidence. Areas of strain maxima tended to be larger in the superior vertebrae when compared with the inferior vertebrae during 4 mm of subsidence. During compression, flexion, axial rotation, and lateral bending, the areas of strain maxima were localized to the area adjacent to the endplate-implant interface. However, during extension, the strain maxima in the superior vertebra was continuous, with the maxima observed near the ALL insertion site.

Discussion

This study evaluated the differences in von Mises strain in the vertebral cancellous bone for PEEK and CoCr implants. Radiolucent PEEK implants provide the ability to
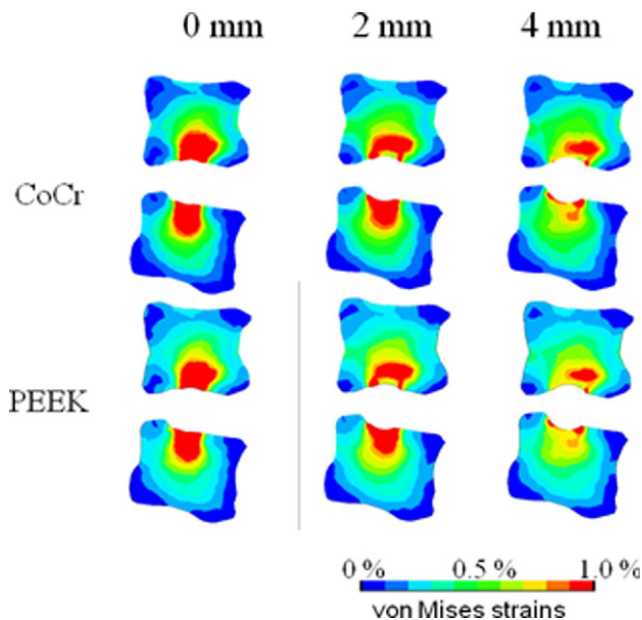
Fig. 5. Effective (von Mises) strain contour plots of L3-4 vertebral bodies at sagittal cut plane for 3 levels of implant subsidence in models implanted with CoCr sphere (top) and models implanted with PEEK implant (bottom).

visualize the surrounding bone and soft tissues during diagnostic imaging, but the biomechanical effects are not fully understood. We hypothesized that the use of a PEEK Fernström prosthesis versus a CoCr prosthesis would have a negligible effect on bone strain. However, we noticed a small reduction in the peak strain values. Results from our study indicated increased peak von Mises strain in the vertebral body cancellous bone for the CoCr implant (14.7%) compared with the PEEK implant (12.9%) when no subsidence of the device was modeled. This is consistent with results from a previous finite element study that documented a reduction in endplate stresses between PEEK and titanium interbody spacers.[47] Those authors concluded that the reduced stresses may result in a lower likelihood of subsidence. However, they did not report stresses in the endplate for an intact scenario. Whereas our study predicted a slight reduction in strain for a PEEK implant, both the PEEK and CoCr implants resulted in a substantial increase in peak strain and area of strain maxima compared with the intact state. In addition, this study indicated that increasing levels of subsidence result in a reduction of the differences between PEEK and CoCr, further suggesting that there may be limited biomechanical advantage to using PEEK for this application. Furthermore, the reductions in peak strain that resulted from increased subsidence or conformity of the endplate to the device still resulted in peak strain much higher than that documented in the intact condition. The results from this study suggest a high subsidence likelihood for either a PEEK or CoCr spherical prosthesis.

Results from this analysis show that implantation of a spherical interbody implant maintains segmental ROM. Initial implantation of the device with no subsidence resulted

in increased ROM for all modes of loading, ranging between 10% and 80% depending on the mode of loading. These results are consistent with previous studies that have evaluated ROM after TDR. Two previous FEM studies indicated increased ROM after implantation of a TDR.[20,22] Similarly, an in vitro cadaveric study also documented increased ROM after TDR during flexion-extension.[48]

Our study documented a progressive reduction in ROM with increased subsidence of the device into the vertebral bodies. Four millimeters of subsidence resulted in decreased ROM for all modes of loading when compared with the intact condition. Interestingly, the greatest increases in ROM at 0 mm of subsidence corresponded to the modes of loading that result in contact of the facets, such as axial rotation, extension, and lateral bending. This suggests that changes in relative facet positioning that occur during distraction had an effect on ROM. Increased subsidence progressively reduced ROM by bringing the facets closer to their preimplantation positioning. This is further corroborated by the fact that flexion, which resulted in no FCF, showed the least sensitivity to subsidence with respect to ROM. These results suggest the need for careful consideration of the amount of surgical distraction required for these types of procedures. A certain amount is required for disc height restoration and neural foraminal decompression, but too much distraction can prevent or limit facet contact. Future work should investigate the effect of ligament and annulus pre-tensioning as a result of distraction. The lack of pre-tensioning in these structures was a limitation of this study but was deemed necessary to control the applied loading. Similarly, smaller implants should be evaluated to determine the effects when subsidence results in a reduction of disc height compared with the intact state.

This study showed similar FCFs between the intact and implanted models. The FCFs progressively increased with increased subsidence of the device. This resulted in increased FCFs for all modes of loading at 4 mm of subsidence. A previous finite element study evaluated the FCF between a fixed and mobile core TDR at varying positions and documented FCFs equivalent to 175% of the intact state depending on positioning and TDR type.[49] This study attributed increases in FCF to a fixed center of rotation of a fixed-core TDR. However, this study applied known physiologic rotations to all of the models instead of loads, thereby negating the potential for increased mobility that arises after TDR,[48] even when one is using a hybrid loading approach.[50] A finite element study that applied loading consistent with bending over to a model implanted with a TDR documented a doubling of the mean facet contact pressure.[20] Similarly, a different finite element study documented the potential for doubling of the FCFs after implantation of a TDR when subjected to rotational loading.[22] Our study documented a maximum increase of FCF of 34%, which occurred during extension and with 4 mm of subsidence of the implant. However, at 2 mm of subsidence, FCFs were decreased by 35% compared with the intact
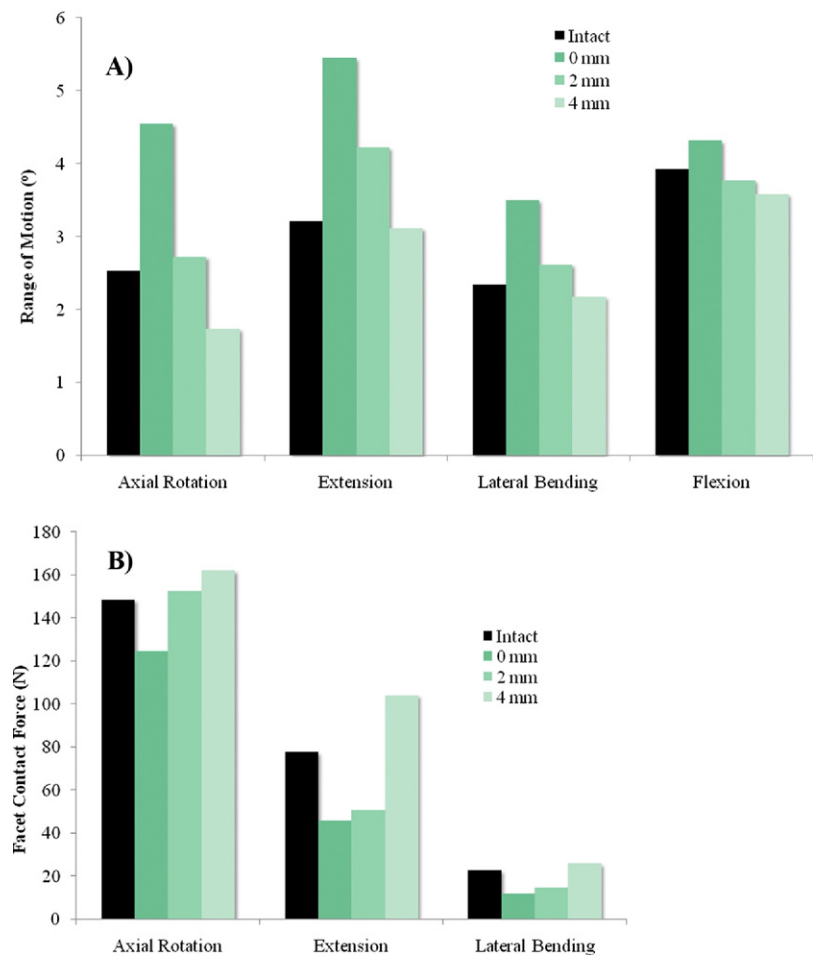
Fig. 6. Bar graphs depicting total angular ROM (A) and total FCF (B) for all loading modes and models.

model during extension. Further examination of the model showed that subsidence of the implant resulted in a reduction in posterior translation of L3 relative to L4 during extension. At 4 mm of subsidence, the total translation was less (2.1 mm) than what was experienced for the intact model (2.41 mm). These results suggest that subsidence of the implant prevents relative translation of the vertebrae, which results in increased loading of the facets. It is difficult to compare the changes in FCFs documented in our study with those reported in previous evaluations of modern TDRs because of the differences in surgical technique. Specifically, implantation of a sphere requires minimal resection of the annulus, which likely helps to maintain preimplantation kinematics and thereby mitigate changes in the facet contact.

This study documented the presence of large areas of strain maxima adjacent to the implant for all modes of loading. We have previously performed a similar analysis on a fixed-core TDR and evaluated the von Mises strains of the cancellous bone.[22] The results of that study indicated that strains typically remained under 1% after implantation, with the exception of a small area during flexion. This is likely the result of the larger contact surface area for a TDR compared with the Fernström sphere, especially at 0 mm of subsidence. This is further indicated by the decreasing area of strain maxima that was observed for increasing levels of subsidence. As the implant nested further into the cancellous bone, the area of contact increased, which resulted in a more distributed load. Even though increased subsidence resulted in reduced areas of strain maxima, the fully nested

Table 2
Percent change in ROM for implanted models compared with intact model

	Axial rotation	Extension	Lateral bending	Flexion
0 mm	80%	70%	50%	10%
2 mm	8%	31%	12%	−4%
4 mm	−32%	−3%	−6%	−9%

Table 3
Percent change in FCF for implanted models compared with intact model

	Axial rotation	Extension	Lateral bending
0 mm	−16%	−41%	−48%
2 mm	3%	−35%	−37%
4 mm	9%	34%	14%

models still depicted strains substantially greater than the intact state. Despite the large areas of strain maxima above 1% documented for all modes of loading, the clinical results depict reasonable levels of subsidence and satisfactory clinical outcomes.[1,13] This suggests that the initial strains experienced by the bone after implantation may not be relevant when one is investigating long-term subsidence of spinal arthroplasty devices. Alternatively, the disparity between the clinical outcomes and high peak strain documented in this study may be explained by increased load bearing in the annulus fibrosus. Specifically, because the Fernström prosthesis maintains the majority of the annulus, continued subsidence may offset the axial loading from the device to the surrounding annulus. The current model did not take this phenomenon into consideration.

In addition, the current model did not account for densification of the underlying bone as a result of the subsidence. This could also act to strengthen the underlying bone and prevent subsequent subsidence, which helps to explain the discrepancy with the reported clinical data. Recent implantations of an interbody sphere by one of the authors (J.I.) has provided radiographic follow-up at 9 months (Fig. 8). This image indicates high signal intensity in the bone adjacent to the implant, suggesting bony remodeling, which

Fig. 8. Coronal computed tomography image of spherical CoCr interbody device implanted at L5-S1. Vertebral bodies show high signal intensity around the implant at 9 months.
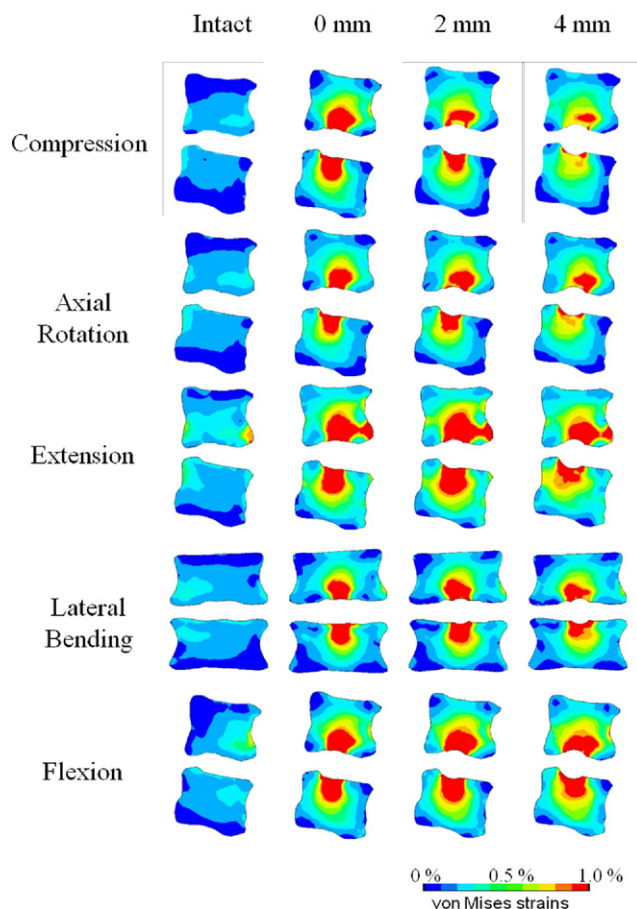
may help to prevent long-term subsidence. However, implantation of TDRs in elderly patients has resulted in severe subsidence,[9] which suggests that good initial bone quality is imperative. Our study further emphasizes the need for a better understanding of the factors attributing to long-term subsidence of spinal implants.

In conclusion, this study evaluated the biomechanical effects of the implantation of a simple spherical interbody implant at 3 levels of subsidence. The results suggest that this simple implant design is able to maintain segmental ROM and provide minimal differences in FCFs. Large areas of von Mises strain were generated in the bone adjacent to the implant regardless of whether the implant was PEEK or CoCr. Despite the large areas of strain documented in this study, clinical results suggest that severe subsidence is not a common complication, and initial subsidence of the device helps secure the device and prevent intervertebral shear translations. However, the disc height loss associated with subsidence may preclude the efficacy of such a device.

Acknowledgments

Fig. 7. Effective (von Mises) strain contour plots of L3-4 vertebral bodies at sagittal or coronal cut plane for all modes of loading and models.

References

1. Fernström U. Arthroplasty with intercorporal endoprothesis in herniated disc and in painful disc. *Acta Chir Scand Suppl* 1966;357:154–9.

2. Wiltberger BR. Surgical treatment of degenerative disease of the back. *J Bone Joint Surg Am* 1963;45:1509–16.

3. Kumar MN, Baklanov A, Chopin D. Correlation between sagittal plane changes and adjacent segment degeneration following lumbar spine fusion. *Eur Spine J* 2001;10:314–9.

4. Pellise F, Hernández A, Vidal X, Minguell J, Martínez C, Villanueva C. Radiologic assessment of all unfused lumbar segments 7.5 years after instrumented posterior spinal fusion. *Spine* 2007;32:574–9.

5. Schulte TL, Leistra F, Bullmann V, et al. Disc height reduction in adjacent segments and clinical outcome 10 years after lumbar 360 degrees fusion. *Eur Spine J* 2007;16:2152–8.

6. Coric D, Mummaneni PV. Nucleus replacement technologies. *J Neurosurg Spine* 2008;8:115–20.

7. Bono CM, Garfin SR. History and evolution of disc replacement. *Spine J* 2004;4(Suppl):145S–50S.

8. Punt IM, Visser VM, van Rhijn LW, Kurtz SM, Antonis J, Schurink GW, van Ooij A. Complications and reoperations of the SB Charite lumbar disc prosthesis: experience in 75 patients. *Eur Spine J* 2008;17:36–43.

9. Bertagnoli R, Yue JJ, Nanieva R, Fenk-Mayer A, Husted DS, Shah RV, Emerson JW. Lumbar total disc arthroplasty in patients older than 60 years of age: a prospective study of the ProDisc prosthesis with 2-year minimum follow-up period. *J Neurosurg Spine* 2006;4:85–90.

10. David T. Long-term results of one-level lumbar arthroplasty: minimum 10-year follow-up of the CHARITE artificial disc in 106 patients. *Spine* 2007;32:661–6.

11. Siepe CJ, Wiechert K, Khattab MF, Korge A, Mayer HM. Total lumbar disc replacement in athletes: clinical results, return to sport and athletic performance. *Eur Spine J* 2007;16:1001–13.

12. Bertagnoli R, Schonmayr R. Surgical and clinical results with the PDN prosthetic disc-nucleus device. *Eur Spine J* 2002;11(Suppl 2):S143–8.

13. McKenzie AH. Intervertebral disc arthroplasty: long-term clinical results. *Orthop Int* 1995;3:313–24.

14. Shim CS, Lee SH, Shin HD, Kang HS, Choi WC, Jung B, Choi G, Ahn Y, Lee S, Lee HY. CHARITE versus ProDisc: a comparative study of a minimum 3-year follow-up. *Spine* 2007;32:1012–8.

15. van Ooij A, Oner FC, Verbout AJ. Complications of artificial disc replacement: a report of 27 patients with the SB Charite disc. *J Spinal Disord Tech* 2003;16:369–83.

16. Siepe CJ, Korge A, Grochulla F, Mehren C, Mayer HM. Analysis of post-operative pain patterns following total lumbar disc replacement: results from fluoroscopically guided spine infiltrations. *Eur Spine J* 2008;17:44–56.

17. Link HD. History, design and biomechanics of the LINK SB Charite artificial disc. *Eur Spine J* 2002;11(Suppl 2):S98–105.

18. Huang RC, Girardi FP, Cammisa FP Jr, Tropiano P, Marnay T. Long-term flexion-extension range of motion of the ProDisc total disc replacement. *J Spinal Disord Tech* 2003;16:435–40.

19. Liu J, Ebraheim NA, Haman SP, Shafiq Q, Karkare N, Biyani A, Goel VK, Woldenberg L. Effect of the increase in the height of lumbar disc space on facet joint articulation area in sagittal plane. *Spine* 2006;31:E198–202.

20. Denoziere G, Ku DN. Biomechanical comparison between fusion of two vertebrae and implantation of an artificial intervertebral disc. *J Biomech* 2006;39:766–75.

21. Rousseau MA, Bradford DS, Bertagnoli R, Hu SS, Lotz JC. Disc arthroplasty design influences intervertebral kinematics and facet forces. *Spine J* 2006;6:258–66.

22. Rundell SA, Auerbach JD, Balderston RA, Kurtz SM. Total disc replacement positioning affects facet contact forces and vertebral body strains. *Spine* 2008;33:2510–7.

23. Kopperdahl DL, Keaveny TM. Yield strain behavior of trabecular bone. *J Biomech* 1998;31:601–8.

24. Mosekilde L, Danielsen CC. Biomechanical competence of vertebral trabecular bone in relation to ash density and age in normal individuals. *Bone* 1987;8:79–85.

25. Hansson TH, Keller TS, Panjabi MM. A study of the compressive properties of lumbar vertebral trabeculae: effects of tissue characteristics. *Spine* 1987;12:56–62.

26. White AA, Panjabi MM. Clinical Biomechanics of the Spine. 2nd ed. Philadelphia: J. B. Lippincott; 1990.

27. Yosibash Z, Padan R, Joskowicz L, Milgrom C. A CT-based high-order finite element analysis of the human proximal femur compared to in-vitro experiments. *J Biomech Eng* 2007;129:297–309.

28. Sawatari T, Tsumura H, Iesaka K, Furushiro Y, Torisu T. Three-dimensional finite element analysis of unicompartmental knee arthroplasty–the influence of tibial component inclination. *J Orthop Res* 2005;23:549–54.

29. Ulrich D, van Rietbergen B, Laib A, Rüegsegger P. The ability of three-dimensional structural indices to reflect mechanical aspects of trabecular bone. *Bone* 1999;25:55–60.

30. Morgan EF, Bayraktar HH, Keaveny TM. Trabecular bone modulus-density relationships depend on anatomic site. *J Biomech* 2003;36:897–904.

31. Kumaresan S, Yoganandan N, Pintar FA, Maiman DJ, Goel VK. Contribution of disc degeneration to osteophyte formation in the cervical spine: a biomechanical investigation. *J Orthop Res* 2001;19:977–84.

32. Silva MJ, Keaveny TM, Hayes WC. Load sharing between the shell and centrum in the lumbar vertebral body. *Spine* 1997;22:140–50.

33. Polikeit A, Nolte LP, Ferguson SJ. The effect of cement augmentation on the load transfer in an osteoporotic functional spinal unit: finite-element analysis. *Spine* 2003;28:991–6.

34. Schmidt H, Heuer F, Simon U, Kettler A, Rohlmann A, Claes L, Wilke HJ. Application of a new calibration method for a three-dimensional finite element model of a human lumbar annulus fibrosus. *Clin Biomech (Bristol, Avon)* 2006;21:337–44.

35. Shirazi-Adl A, Ahmed AM, Shrivastava SC. Mechanical response of a lumbar motion segment in axial torque alone and combined with compression. *Spine* 1986;11:914–27.

36. Rohlmann A, Zander T, Schmidt H, Wilke HJ, Bergmann G. Analysis of the influence of disc degeneration on the mechanical behaviour of a lumbar motion segment using the finite element method. *J Biomech* 2006;39:2484–90.

37. Schmidt H, Heuer F, Drumm J, Klezl Z, Claes L, Wilke HJ. Application of a calibration method provides more realistic results for a finite element model of a lumbar spinal segment. *Clin Biomech (Bristol, Avon)* 2007;22:377–84.

38. Noailly J, Lacroix D, Planell JA. Finite element study of a novel intervertebral disc substitute. *Spine* 2005;30:2257–64.

39. Frei H, Oxland TR, Rathonyi GC, Nolte LP. The effect of nucleotomy on lumbar spine mechanics in compression and shear loading. *Spine* 2001;26:2080–9.

40. Yamamoto I, Panjabi MM, Crisco T, Oxland T. Three-dimensional movements of the whole lumbar spine and lumbosacral joint. *Spine* 1989;14:1256–60.

41. Mimura M, Panjabi MM, Oxland TR, Crisco JJ, Yamamoto I, Vasavada A. Disc degeneration affects the multidirectional flexibility of the lumbar spine. *Spine* 1994;19:1371–80.

42. Panjabi MM, Oxland TR, Yamamoto I, Crisco JJ. Mechanical behavior of the human lumbar and lumbosacral spine as shown by three-dimensional load-displacement curves. *J Bone Joint Surg Am* 1994;76:413–24.

43. Fujiwara A, Lim TH, An HS, Tanaka N, Jeon CH, Andersson GB, Haughton VM. The effect of disc degeneration and facet joint osteoarthritis on the segmental flexibility of the lumbar spine. *Spine* 2000;25:3036–44.

44. Schmoelz W, Huber JF, Nydegger T, Claes L, Wilke HJ. Dynamic stabilization of the lumbar spine and its effects on adjacent segments: an in vitro experiment. *J Spinal Disord Tech* 2003;16:418–23.

45. Niosi CA, Zhu QA, Wilson DC, Keynan O, Wilson DR, Oxland TR. Biomechanical characterization of the three-dimensional kinematic

behaviour of the Dynesys dynamic stabilization system: an in vitro study. *Eur Spine J* 2006;15:913–22.

46. Nagaraja S, Couse TL, Guldberg RE. Trabecular bone microdamage and microstructural stresses under uniaxial compression. *J Biomech* 2005;38:707–16.

47. Vadapalli S, Sairyo K, Goel VK, Robon M, Biyani A, Khandha A, Ebraheim NA. Biomechanical rationale for using polyetheretherketone (PEEK) spacers for lumbar interbody fusion—a finite element study. *Spine* 2006;31:E992–8.

48. O'Leary P, Nicolakis M, Lorenz MA, Voronov LI, Zindrick MR, Ghanayem A, Havey RM, Carandang G, Sartori M, Gaitanis IN, Fronczak S, Patwardhan AG. Response of Charite total disc replacement under physiologic loads: prosthesis component motion patterns. *Spine J* 2005;5:590–9.

49. Moumene M, Geisler FH. Comparison of biomechanical function at ideal and varied surgical placement for two lumbar artificial disc implant designs: mobile-core versus fixed-core. *Spine* 2007;32:1840–51.

50. Goel VK, Grauer JN, Patel TCh, Biyani A, Sairyo K, Vishnubhotla S, Matyas A, Cowgill I, Shaw M, Long R, Dick D, Panjabi MM, Serhan H. Effects of Charite artificial disc on the implanted and adjacent spinal segments mechanics using a hybrid testing protocol. *Spine* 2005;30:2755–64.